PCCP

Accepted Manuscript

This is an *Accepted Manuscript*, which has been through the Royal Society of Chemistry peer review process and has been accepted for publication.

Accepted Manuscripts are published online shortly after acceptance, before technical editing, formatting and proof reading. Using this free service, authors can make their results available to the community, in citable form, before we publish the edited article. We will replace this *Accepted Manuscript* with the edited and formatted *Advance Article* as soon as it is available.

You can find more information about *Accepted Manuscripts* in the Information for Authors.

Please note that technical editing may introduce minor changes to the text and/or graphics, which may alter content. The journal's standard Terms & Conditions and the Ethical guidelines still apply. In no event shall the Royal Society of Chemistry be held responsible for any errors or omissions in this *Accepted Manuscript* or any consequences arising from the use of any information it contains.

ROYAL SOCIETY OF CHEMISTRY

www.rsc.org/pccp

From Two-Dimension to One-Dimension: Curvature Effect of Silicon-Doped Graphene and Carbon Nanotubes for Oxygen Reduction Reaction

Peng Zhang[1,3], Xiuli Hou[1,*], Jianli Mi[1], Yanqiong He[1], Lin Lin,[4] Qing Jiang,[3] and Mingdong Dong[2,*]

[1] *Institute for Advanced Materials, and School of Materials Science and Engineering, Jiangsu University, Zhenjiang 212013, China.*

[2] *Center for DNA Nanotechnology (CDNA), interdisciplinary Nanoscience Center (iNANO), Aarhus University, DK-8000 Aarhus, Denmark.*

[3] *Key Laboratory of Automobile Materials, Ministry of Education, and Department of Materials Science and Engineering, Jilin University, Changchun 130022, China.*

[4] *School of Food & Biological Engineering, Jiangsu University, Zhenjiang 212013, China.*

Abstract

For the goal of practical industrial development of fuel cells, inexpensive, sustainable, and high efficient electrocatalysts for oxygen reduction reactions (ORR) are highly desirable alternatives to platinum (Pt) and other rare metals. In this work, based on density functional theory, silicon (Si)-doped carbon nanotubes (CNTs) and graphene as metal-free, low cost, and high-performcance electrocatalysts for ORR are studied systematically. It is found that curvature effect plays an important role in the adsorption and reduction of oxygen. The adsorption of O_2 becomes weaker as the curvature varies from positive values (outside CNTs) to negative values (inside CNTs).

* Corresponding author. Email: houxiuli@ujs.edu.cn, dong@inano.au.dk

Physical Chemistry Chemical Physics Accepted Manuscript

The free energy change of the rate-determining step of ORR on concave inner surface of Si-doped CNTs is smaller than that on the counterpart of Si-doped graphene, while that on convex outer surface of Si-doped CNTs is larger than that on Si-doped graphene. Uncovering this new ORR mechanism on silicon-doped carbon electrodes is significant as the same principle could be applied to the development of various other metal-free efficient ORR catalysts for fuel cell applications.

Keywords: silicon-doped graphene, silicon-doped carbon nanotubes, fuel cell, oxygen reduction reaction

Physical Chemistry Chemical Physics Accepted Manuscript

1. Introduction

Fuel cells and metal-air batteries have attracted much interest due to their high efficiency and low environmental impact. The sluggish kinetics of the oxygen reduction reaction (ORR) at the cathode is one of the key factors limiting the performance of fuel cells and metal-air batteries. How to facilitate ORR with proper catalysts is a key issue to date. The state-of-the-art catalyst is based on precious metal Pt.[1,2] However, the high costs, limited resources, and poor durability of Pt catalyst precludes the commercialization of these technologies. Therefore, developing advanced and cheaper cathode catalysts has been a foremost field in chemistry. In the past decade, significant progress has been made in finding alternative electrocatalysts for ORR, including Pt-transition-metal alloys,[3-5] core-shell nanoparticles,[6,7] metal macrocycles,[8,9] metal oxides,[10,11] and metal-free heteroatoms doped carbon materials.[12-16]

Carbon materials doped with heteroatoms have been shown pronounced catalytic activity and long-term operation stability. N-doped carbon materials with a graphitic structure, such as carbon nanotubes (CNTs) and graphene, can act as promising candidates to replace Pt-based catalysts, because they not only exhibit a four-electron ORR process with a 3-time higher electrocatalytic activity than that of commercially available Pt-based electrodes in alkanline electrolytes, but also possess long-term stability and excellent methanol and CO tolerance.[17,18] P-doped graphite layers, S-doped graphene, B-doped CNTs and F-doped carbon blacks have also shown pronounced catalytic activity.[19-22] Especially, binary and ternary doping carbon

Physical Chemistry Chemical Physics Accepted Manuscript

materials exhibit superior catalytic activity than corresponding single doped counterparts.[23-27] Both theoretical calculations and detailed experiments have confirmed that the improved electrocatalytic activity of carbon materials can be attributed to the change of the electronic structures by introducing dopant atoms into graphite lattice, which are favorable for O_2 adsorption,[28,29] resulting in enhanced ORR activity, regardless of the dopant atom. It has been proved that the graphene doped by substitution of the C atom by N/B atoms behaves as an *n*/*p*-doped material.[30] N-doped graphene has a lower workfunction value (3.10 eV) compared with pristine graphene, while that of B-doped graphene is increased to the value of 5.57 eV.[30]

It has been shown that the catalytic activity of catalysts depends on their composition, size, structure and shape, et al.[31-33] In this contribution, ORR on Si-doped graphene and CNTs, which exhibit good stability and electronic properties,[34-37] have been studied systematically. Our results show that O_2 adsorption and reduction depend on the curvature of the catalysts. Both the adsorption energies (E_{ad}) of O_2 and the free energy changes (ΔG) of the rate-determining step involved in ORR become larger as the curvature changes from negative to positive.

2. Computational Method

Spin-polarized density functional theory (DFT) calculations are carried out by using DMol^3 code.[38,39] The electron exchange-correlation potentials are described by the generalized gradient approximation (GGA) with Perdew-Burke-Ernzerhof (PBE) function.[40] PBE is the most common density functional in chemistry and materials science. However, it suffers some of the shortcomings of the classical DFT

Physical Chemistry Chemical Physics Accepted Manuscript

functionals such as self-interaction error and failure to accurate describe the van der Waals forces.[41] Therefore, a Grimme approach is adopted for dispersion corrections.[42] The core treatment parameter controls how electrons in the lowest lying atomic orbitals are treated. With heavier elements, relativistic effects become important in the core electrons. Here, the all electron relativistic (AER) method is implemented for core treat, which includes all electrons explicitly and introduces some relativistic effects into the core.[43] As the name implies, the core electrons are still included in the calculation, but scalar relativistic effects are included. This technique initially omits the spin-orbit interaction (thus keeping spin as a good quantum number), but retains all other relativistic kinematic effects such as mass-velocity, Darwin, and higher order terms.[43] Coupled first-order differential equations are solved which do not involve derivatives of the potential. The spin-orbit interaction can be included as a perturbation once the ′relativistic′ spin-polarized bands and wavefunctions have been obtained.[43] The double numerical plus polarization (DNP) is specified as the atomic orbital basis set.[38] A smearing of 0.005 Ha (1 Ha = 27.21 eV) to the orbital occupation is applied to achieve accurate electronic convergence. In order to ensure high-quality results, the real-space global orbital cutoff radius is chosen to be as high as 4.6 Å. The structure optimization is an iterative procedure until the convergence tolerances are reached. The convergence tolerance of energy, maximum force and displacement are 1.0×10^{-5} Ha, 0.002 Ha/Å and 0.005 Å, respectively. The transition state (TS) for O_2 dissociation is obtained by LST/QST tools in DMol^3 code.[44,45]

In this work, both Si-doped graphene and CNTs are considered. For Si-doped

Physical Chemistry Chemical Physics Accepted Manuscript

graphene, all simulations are performed in a 6 × 6 graphene supercell, including 72 atoms. The minimal distance between the graphene sheet and its mirror images is set as large as 15 Å, which is sufficiently large to avoid the interaction between them. For Si-doped CNTs, the supercell models include three unit cells of (10, 0) tubes. The orthorhombic supercell is constructed as 30 × 30 × 12.78 $Å^3$. Two Si-doped structures are considered here, including single vacancy (V_S) and divacancy (V_D) sites,[34,35] as shown in Fig. 1. The E_{ad} of adsorbates on Si-doped graphene and CNTs are calculated by $E_{ad} = E_{ads} + E_{sub} - E_{ads/sub}$, where E_{ads}, E_{sub} and $E_{ads/sub}$ are the electronic energies of an isolated adsorbate molecule, Si-doped graphene or CNTs, and the adsorption systems, respectively. By these definitions, the positive adsorption energy values correspond to the exothermic adsorption processes. The H_2O solvent environment is simulated by a conductor-like screening model (COSMO).[46] The COSMO is a continuum model in which the solute molecule forms a cavity within the dielectric continuum of permittivity.[46] The DMol^3/COSMO method has been generalized to the periodic boundary cases.[46] The deviation of the COSMO approximation from the exact solution is very small. For strong dielectrics like H_2O, it is less than 1%. The dielectric constant is selected as 78.54 for H_2O solvent.

It is known that ORR mechanisms at cathodes in acidic and alkaline solutions are different. In acidic media , the electrode reaction can be expressed in O_2 dissociation mechanism $O_2 + 4H^+ + 4e^- \rightarrow 2O + 4H^+ + 4e^- \rightarrow 2OH^- + 2H^+ + 2e^- \rightarrow 2H_2O$ or OOH association mechanism $O_2 + 4H^+ + 4e^- \rightarrow OOH + 3H^+ + 3e^- \rightarrow O + H_2O + 2H^+ + 2e^- \rightarrow OH + H^+ + e^- + 2H_2O \rightarrow 2H_2O$, while that in alkaline media can be written

Physical Chemistry Chemical Physics Accepted Manuscript

as $O_2 + 2H_2O + 4e^- \rightarrow O + 2OH^- + H_2O + 2e^- \rightarrow 4OH^-$.[47-49] The complete electrochemical ORR involves four net coupled proton and electron transfer steps to O_2 molecule at the cathode. Proton transfer is coupled with electron transfer as well. Barriers for electrochemical proton transfers have been calculated for the reduction of O_2 to OOH and OH to H_2O on Pt(111) surface and Fe/N/C catalysts.[50-52] In all cases, the calculated proton-transfer reaction barriers are small (0.15 eV to 0.25 eV), and diminish with higher applied voltages. At a first approximation, we expect that barriers for electrochemical proton transfers to adsorbed intermediates in this study will be small and easily surmountable at room temperature. As a result, we only calculate the reaction energy for every elemental step. Free energies of the ORR intermediates can be calculated based on a computational hydrogen electrode (CHE) model suggested by Nørskov et al.[53,54] The change of free energy for elemental step involving coupled proton and electron transfer is determined as follows: $\Delta G = \Delta E + \Delta ZPE - T\Delta S + \Delta G_{pH} + \Delta G_U$, where ΔE is the reaction energy based on DFT calculation, ΔZPE is the zero point energy, T is temperature and ΔS is the change in the entropy, ΔG_{pH} and ΔG_U are the free energy contributions due to variations in pH value and electrode potential U, respectively. Zero point energy and entropy of the ORR intermediates are calculated based on the vibrational frequencies. The effect of electrode potential U for all the states involving electron and proton transfer is determined by $\Delta G_U = -neU$, where n is number of electrons transferred and U is the electrode potential.[55] For pH differing from 0, pH effect is obtained by $\Delta G_{pH} = -k_B T \ln[H^+] = pH \times k_B T \ln 10$. In this work, pH value is assumed to be 0 for acidic

Physical Chemistry Chemical Physics Accepted Manuscript

medium and 14 for alkaline medium.

3. Results and Discussion

3.1 Oxygen Reduction Reaction (ORR) on Si-Doped Graphene. The adsorption characteristics of five intermediates on Si-doped graphene are listed in Table 1 and Fig. 1. Similar to that on layered SiC sheets, the active site of Si-doped carbon materials locates on the Si atoms, due to the smaller electronegativity of Si atom compared with C atom.[47] All the intermediates involved in ORR adsorb at or near Si atom. O_2 prefers to adsorb on V_D site as end-on configuration with E_{ad} of 0.57 eV, which is 0.23 eV larger than that with side-on configuration. This is consistent with O_2 adsorption on Fe/N/C catalyst and metal phthalocyanine.[56,57] The O-O bond length of the adsorbed O_2 are elongated nearly 0.156 Å due to the electronic charge transfer from Si atom to O_2-2π* orbital. The charge transfer from Si atom to O_2 is quantified to be 0.461 *e* according to Hirshfeld population analysis. Not that the interaction energy E_{int} ($E_{int} = E_{ads}' + E_{sub}' - E_{ads/sub}$, where E_{ads}' and E_{sub}' are the energies of adsorbate molecule and substrate already in its deformed geometry, respectively.) is as high as 1.61 eV, which compensate to the relaxation of the Si-doped graphene. The most favorable adsorption site for O atom is the bridge site near Si atom, giving rise to an epoxide-like structure with E_{ad} value of 5.27 eV, which is 0.90 eV larger than that on the next most stable one of atop site on Si atom. OH, OOH and H_2O tend to adsorb at atop site of Si atom other than C atom with E_{ad} values of 3.59, 1.88 and 0.45 eV, respectively.

Compared with that on V_D site, the favorable adsorption configurations of ORR

Physical Chemistry Chemical Physics Accepted Manuscript

intermediates on V_S site are similar except for O_2 molecule and O atom. The most energetically favorable configuration of O_2 on V_S site is characterized by O_2 parallel to the graphene surface forming two chemical bonds with the Si atom (side-on) with E_{ad} of 2.35 eV. O atom tends to adsorb at atop site of Si atom with E_{ad} of 6.24 eV rather than bridge site. Note that the adsorption energies of ORR intermediates on V_S site are much larger than that on V_D site. The E_{ad} values of OH, OOH and H_2O at V_S site are 4.83, 3.08 and 0.84 eV, respectively. The stronger adsorption of these intermediates promotes the initial O_2 adsorption step on V_S site; however, it may hinder further reaction steps toward oxygen reduction due to potentially increased energy barriers. The strong binding interaction of ORR intermediates on V_S site may cause the proton/electron-transfer steps to be strongly endothermic, thereby hindering the formation of product species no matter in acidic media or in alkaline media, as shown in Fig. 2. Thus, ORR on V_S site is not considered further in this work.

ORR in acidic media is considered firstly. Fig. 3 shows a comparison of the ORR mechanisms between the O_2 dissociation mechanism and OOH association mechanism, which indicates that ORR in OOH association mechanism exhibits relatively low free energy barriers. O_2 dissociation is the rate-determining step in O_2 dissociation mechanism at low potential. The energy barrier of O_2 dissociation is 0.86 eV, which is too large to overcome at room temperature and prevents the further reduction steps of ORR. After further considering the van der Waals attraction, it is found that the adsorption of O_2 is enhanced, while the barrier for O_2 dissociation is barely changed, as shown in Table 2. By contrast, the energy barriers of OOH

Physical Chemistry Chemical Physics Accepted Manuscript

formation and OOH combined with H to form O and H_2O are easy to cross, and the ΔG values of these two elemental steps are calculated to be −1.34 and −2.77 eV at zero potential (U = 0V vs. the RHE), respectively. The rate-determining step of OOH association mechanism lies in the last proton/electron transfer step of H_2O formation with ΔG increasing from 0.31 eV at U = 0 V to 1.54 eV at U = 1.23 V. Note that the value of ΔG for the rate-determining step can be used as a measure of the reaction rate.[58] The smaller the ΔG value is, the faster the corresponding reaction step.[58] The high endothermic ΔG value of H_2O formation on V_D site indicates that the ORR catalytic activity of Si-doped graphene is very poor.

A substantially different picture is obtained for ORR under alkaline environment, as shown in Fig. 3(c). At U = 0 V, the ΔG values of two elemental steps (adsorbed O_2 molecule reaction with H_2O and O atom reaction with H_2O) are −2.54 and 0.94 eV, respectively. When an ideal electrode potential of 0.40 V is applied, the energy level of energy double proton/electron transfer step is shifted up by 0.80 eV. O_2 molecule reaction with H_2O is exothermic with ΔG of −1.74 eV, while O atom reaction with H_2O is endothermic with ΔG of 1.74 eV. The ΔG of the later step is the largest one among all the elemental steps, which is too large to overcome and implies that this step is the most sluggish one and represents the highest resistance for the whole ORR.

3.2 Oxygen Reduction Reaction (ORR) on Si-doped CNTs. In this work, ORR on concave inner and convex outer surface of Si-doped CNTs with V_D defect site is considered. It is found that in the case of convex outer surface, O_2 adsorption is significantly enhanced compared with that on Si-doped graphene, while the

Physical Chemistry Chemical Physics Accepted Manuscript

adsorption of O_2 is reduced on concave inner surface, as shown in Fig. 4. From these observations, it can be concluded that the binding strength of ORR intermediates is strongly dependent on the curvature. The variation of adsorption may be exploited to the morphological transformations. The curvature of CNT walls causes the electron density of the graphene layers to shift from the concave inner to the convex outer surface, resulting in the asymmetric distribution of charge and an electric potential difference.[59] The larger the curvature, the more electron transfer from concave inner to the convex outer surface is, bringing out different adsorption properties of O_2 inside and outside Si-doped CNTs. Due to the different adsorption properties, energy diagram of ORR on Si-doped CNTs is quite different from that on Si-doped graphene.

We take (10, 0) CNT as an example to study the ORR progress. Fig. 5 shows the energy diagrams of ORR in OOH association mechanism on convex outer and concave inner surface of Si-doped (10, 0) CNT with V_D defect site, which differ from that on Si-doped graphene. The ΔG values of four proton/electron transfer steps involved in ORR in acidic media on convex outer surface of Si-doped (10, 0) CNT with V_D defect site are −1.44 eV for OOH formation, −3.04 eV for OOH reaction H, −0.74 eV for OH formation, and 0.83 eV for H_2O formation at U = 0 V, while the ΔG values of the four elemental steps on concave inner surface are −0.80, −2.32, −1.63 and −0.40 eV, respectively. Similar with that on Si-doped graphene, ΔG of H_2O formation is the largest one among the four reaction steps on convex outer and concave inner surfaces of Si-doped CNT, which indicates that this step represents the highest resistance for the whole ORR. As electrode potential U increases from 0 V to

Physical Chemistry Chemical Physics Accepted Manuscript

1.23 V, energy level is shifted for each proton/electron transfer step. At U = 1.23 V, H_2O formation on convex outer surface is endothermic with ΔG of 2.06 eV, which is larger than that on Si-doped graphene due to the stronger adsorption of OH, suggesting unfavorable catalytic activity. However, ΔG value of H_2O formation on concave inner surface is 0.83 eV at U = 1.23 V, which is smaller than that on Si-doped graphene (1.54 eV), indicating favored catalytic activity. This result also suggests that an ORR mechanism involving stronger binding of O* and OH* intermediates requires higher overpotentials for oxygen reduction. This remarkable change in the ΔG of rate-determining step indicates that the stability of the ORR intermediates serves a key role in the activity of catalyst toward oxygen reduction as previously discussed.[60,61] In addition, concave inner surface of CNTs support significantly contributes to the reduction of the energy barrier, which provides an opportunity for tuning the activity of carbon materials by using curvature.

Similar with that in acidic media, ORR on concave inner surface is favorable than that on convex outer surface and graphene in alkaline. The ΔG value of O_2 molecule reaction with H_2O and that of O atom reaction with H_2O on concave inner surface are determined to be −1.46 and −0.38 eV at U = 0 V, and −0.66 and 0.42 eV at U = 0.40 V. By comparison, the ΔG values of O_2 reaction with H_2O and O atom reaction with H_2O on convex outer surface are calculated to be −2.82 and 1.75 eV at U = 0V, and −2.02 and 2.55 eV at U = 0.40 V. The lower ΔG value of the rate-determining step for the concave inner surface compared to the convex outer surface and graphene potentially results in a faster kinetics property.

Physical Chemistry Chemical Physics Accepted Manuscript

According to the developed theories of catalyst surfaces, the ORR electrocatalytic activity of a given catalyst is governed by the E_{ad} of ORR intermediates.[58,61,62] The magnitudes of ΔG during the ORR are related to the stability of adsorbed OOH, O and OH. As shown in Fig. 6, the adsorption of the OH, OOH and H_2O intermediates on Si-doped graphene and CNTs scale roughly with the stability of adsorbed O. The E_{ad} of O can be used to characterize the reaction barriers of ORR in both acidic and alkaline environments. If E_{ad} of O becomes increasingly weaker, ΔG values for O and OH removal decrease because it becomes easier to break the Pt-OH and Pt-O bonds. It is clear that ΔG decreases with the decreasing of E_{ad} of O as shown in Fig. 6. Concave inner surface of CNTs exhibits best catalytic activity no matter in acidic media or alkaline media due to the optimum adsorption characterize of ORR intermediates.

The above results show that the adsorption of ORR intermediates and free energy changes during ORR process on Si-doped graphene and CNTs display curvature effect. Namely, the catalytic activity of ORR on Si-doped carbon materials can be adjusted by the curvature. Our discussion about curvature effect of ORR may be especially significant in porous carbon materials, which can yield the advantage of negative curvature.

4. Conclusions

On the basis of the first principles calculations, ORR on Si-doped graphene and CNTs are studied. It is found that O_2 adsorption and reduction exhibit curvature effect. The E_{ad} of O_2 and the ΔG of the rate-determining step in ORR become smaller as the

Physical Chemistry Chemical Physics Accepted Manuscript

curvature varies from a positive one (outside CNT) to a negative one (inside CNT). These results are believed to be significant because they not only give further insight into the ORR mechanism on these metal-free heteroatom doped carbon materials, but also open a new way to fabricate new low-cost nonprecious-metal catalysts with high electrocatalytic activity for fuel cells applications.

Acknowledgments

We acknowledge the financially supported by Natural Science Foundation of Jiangsu (No. SBK201341900 and BK2011468), National Natural Science Foundation of China (301101388), China Postdoctoral Science Foundation (No. 2013M541611 and 2014M550270), and the Senior Intellectuals Fund of Jiangsu University (No. 12JDG094 and 13JDG032).

Physical Chemistry Chemical Physics Accepted Manuscript

Table 1. Adsorption energy (E_{ad}) values of ORR intermediates on Si-doped graphene and (10, 0) CNT with V_S and V_D defect sites. All results are in unit of eV.

E_{ad}	O_2	OH	O	H_2O	OOH
V_S-graphene	2.35	4.83	6.24	0.84	3.08
V_D-CNT outside	1.00	4.11	6.02	0.90	2.38
V_D-graphene	0.57	3.59	5.27	0.45	1.88
V_D-CNT inside	0.25	2.71	3.76	−0.10	1.02

Table 2. Comparison of O_2 adsorption and dissociation on Si-doped graphene with and without van der Waals bonding. E_{ad}, E_a and E_r stand for the adsorption energy, barrier energy and reaction energy, respectively. All results are in unit of eV.

	E_{ad}	E_a	E_r
V_S-graphene	2.35 (2.48)[a]	0.62 (0.58)	−0.49 (−0.53)
V_D-graphene	0.57 (0.72)	0.86 (0.84)	−2.53 (−2.56)

[a] The energies if parenthesis are calculated under the consideration of van der Waals force.

Physical Chemistry Chemical Physics Accepted Manuscript

Captions

Fig. 1. Optimized adsorption structures of the ORR intermediates on (O_2, O, OOH, OH and H_2O) Si-doped graphene with V_D defect site (a) and V_S defect site (b).

Fig. 2. Free energy diagrams of ORR on Si-doped graphene with V_S defect site in acidic media (a) and alkaline media (b).

Fig. 3. Free energy diagrams of ORR on Si-doped graphene with V_D defect site: (a) ORR in acidic media through O_2 dissociation mechanism; (b) ORR in acidic media through OOH association mechanism; (c) ORR in alkaline media. (d) atomic configurations of O_2 dissociation on Si-doped graphene with V_D defect site, including initial state (IS), transition state (TS) and final state (FS).

Fig. 4. (a) Preferred adsorption structures of O_2 adsorbed on concave inner and convex outer surfaces of Si-doped (10,0) CNT with V_D defect site; (b) adsorption energies (E_{ad}) of O_2 on Si-doped graphene and CNTs with V_D defect site.

Fig. 5. Free energy diagrams of ORR on concave inner surface (a, b) and convex outer surface (c, d) of Si-doped (10,0) CNT with V_D defect site under acidic media (a, c) and alkaline media (b, d).

Fig. 6. The ΔG values of the rate-determining step (RDS) involved in ORR under acidic media and the adsorption energies (E_{ad}) of OH, OOH and H_2O plotted against the adsorption energy of O (E_{ad}-O) for Si-doped (10,0) CNT with V_D defect site.

Physical Chemistry Chemical Physics Accepted Manuscript

Fig. 1.

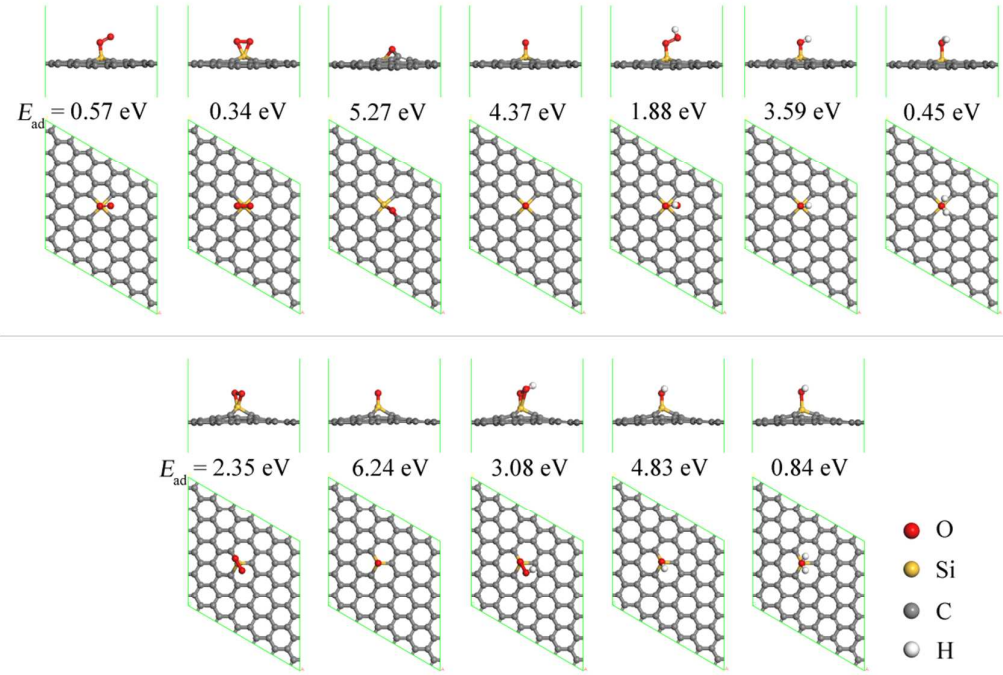

Fig. 2.

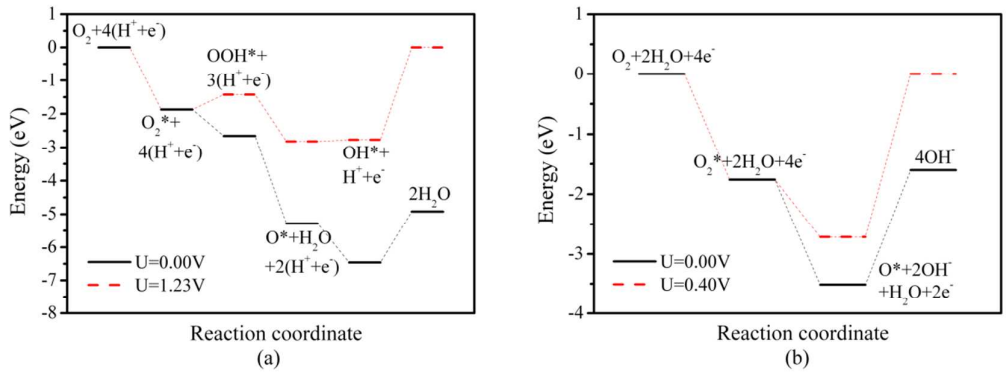

Physical Chemistry Chemical Physics Accepted Manuscript

Fig. 3.

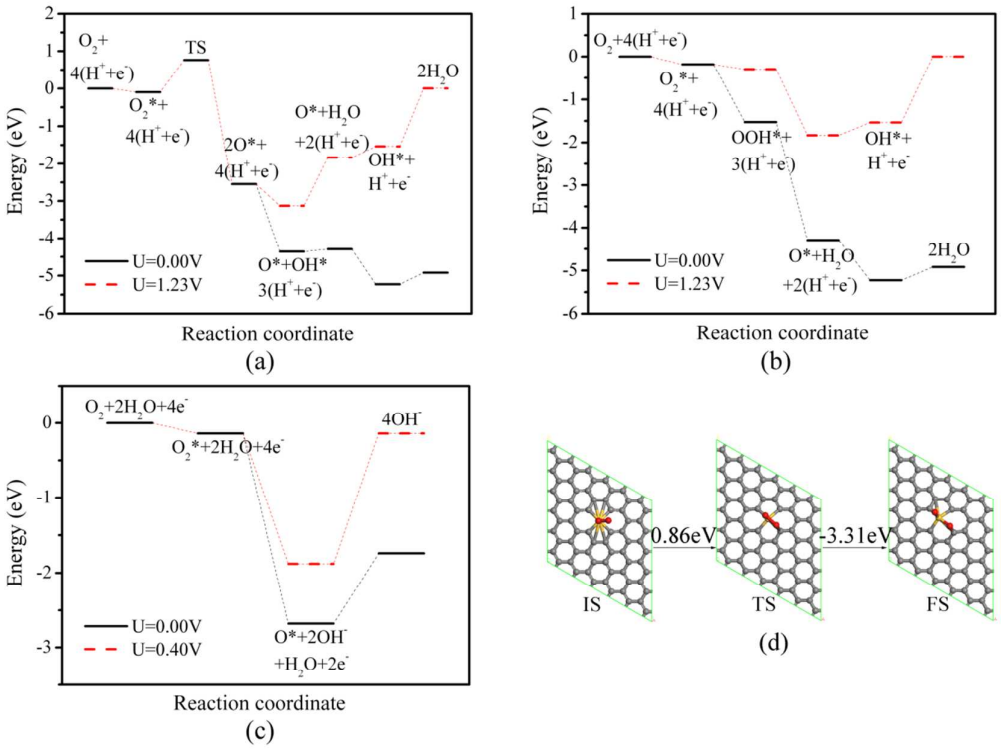

Fig. 4.

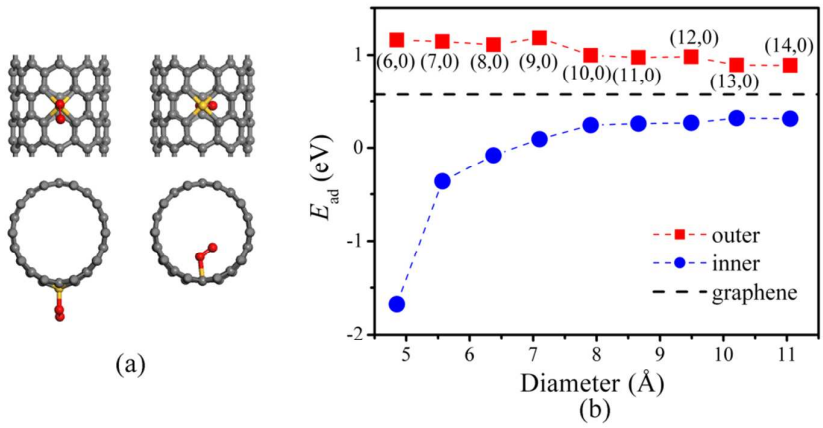

Physical Chemistry Chemical Physics Accepted Manuscript

Fig. 5.

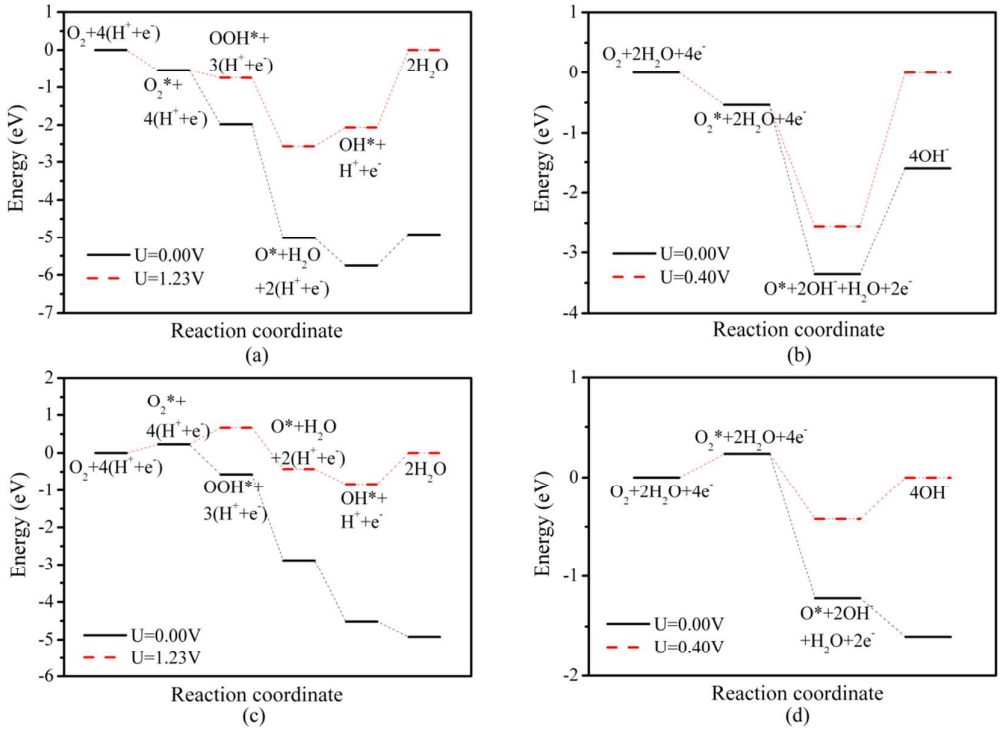

Fig. 6.

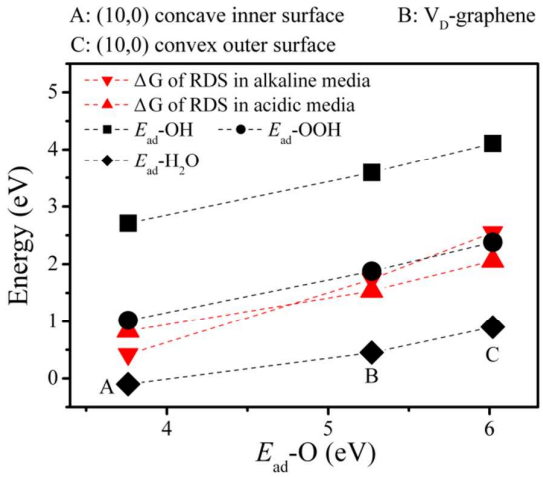

Physical Chemistry Chemical Physics Accepted Manuscript

Physical Chemistry Chemical Physics Accepted Manuscript

References

1. H. A. Gasteiger, S. S. Kocha, B. Sompalli and F. T. Wagner, *Appl. Catal. B*, 2005, **56**, 9-35.
2. X. Yu and S. Ye, *J. Power Sources*, 2007, **172**, 145-154.
3. V. R. Stamenkovic, B. S. Mun, M. Arenz, K. J. Mayrhofer, C. A. Lucas, G. Wang, P. N. Ross and N. M. Markovic, *Nat. Mater.*, 2007, **6**, 241-247.
4. C. Wang, D. Li, M. Chi, J. Pearson, R. B. Rankin, J. Greeley, Z. Duan, G. Wang, D. van der Vliet, K. L. More, N. M. Markovic and V. R. Stamenkovic, *J. Phys. Chem. Lett.*, 2012, 1668-1673.
5. C. Wang, N. M. Markovic and V. R. Stamenkovic, *ACS Catal.*, 2012, 891-898.
6. P. Strasser, S. Koh, T. Anniyev, J. Greeley, K. More, C. Yu, Z. Liu, S. Kaya, D. Nordlund, H. Ogasawara, M. F. Toney and A. Nilsson, *Nat. Chem.*, 2010, **2**, 454-460.
7. R. Srivastava, P. Mani, N. Hahn and P. Strasser, *Angew. Chem. Int. Ed.*, 2007, **46**, 8988-8991.
8. J. P. Collman, N. K. Devaraj, R. A. Decreau, Y. Yang, Y. L. Yan, W. Ebina, T. A. Eberspacher and C. E. D. Chidsey, *Science*, 2007, **315**, 1565-1568.
9. J. D. Baran, H. Grönbeck and A. Hellman, *J. Am. Chem. Soc.*, 2013, **136**, 1320-1326.
10. H. T. Chung, J. H. Won and P. Zelenay, *Nat. Commun.*, 2013, **4**, 1922.
11. Y. Gorlin, C. J. Chung, D. Nordlund, B. M. Clemens and T. F. Jaramillo, *ACS Catal.*, 2012, 2687-2694.

12. X. Sun, P. Song, Y. Zhang, C. Liu, W. Xu and W. Xing, *Sci. Rep.*, 2013, **3**, 2505.

13. Q. Shi, F. Peng, S. Liao, H. Wang, H. Yu, Z. Liu, B. Zhang and D. Su, *J. Mater. Chem. A*, 2013, **1**, 14853-14857.

14. H. Wang, T. Maiyalagan and X. Wang, *ACS Catal.*, 2012, **2**, 781-794.

15. C. Zhu and S. Dong, *Nanoscale*, 2013, **5**, 1753-1567.

16. H. Kim, K. Lee, S. I. Woo and Y. Jung, *Phys. Chem. Chem. Phys.*, 2011, **13**, 17505-17510.

17. K. Gong, F. Du, Z. Xia, M. Durstock and L. Dai, *Science*, 2009, **323**, 760-764.

18. L. Qu, Y. Liu, J.B. Baek and L. Dai, *ACS Nano*, 2010, **4**, 1321-1326.

19. Z. W. Liu, F. Peng, H. J. Wang, H. Yu, W. X. Zheng and J. Yang, *Angew. Chem. Int. Ed.*, 2011, **50**, 3257-3261.

20. L. Yang, S. Jiang, Y. Zhao, L. Zhu, S. Chen, X. Wang, Q. Wu, J. Ma, Y. Ma and Z. Hu, *Angew. Chem. Int. Ed.*, 2011, **50**, 7132-7135.

21. X. Sun, Y. Zhang, P. Song, J. Pan, L. Zhuang, W. Xu and W. Xing, *ACS Catal.*, 2013, **3**, 1726-1729.

22. Z. Yang, Z. Yao, G. Li, G. Fang, H. Nie, Z. Liu, X. Zhou, X. a. Chen and S. Huang, *ACS Nano*, 2011, **6**, 205-211.

23. S. Wang, L. Zhang, Z. Xia, A. Roy, D. W. Chang, J. B. Baek and L. Dai, *Angew. Chem. Int. Ed.*, 2012, **51**, 4285-4288.

24. C. H. Choi, S. H. Park and S. I. Woo, *ACS Nano*, 2012, **6**, 7084-7091.

25. Y. Zheng, Y. Jiao, L. Ge, M. Jaroniec and S. Z. Qiao, *Angew. Chem. Int. Ed.*, 2013, **52**, 3110-3116.

Physical Chemistry Chemical Physics Accepted Manuscript

26. D. Yu, Y. Xue and L. Dai, *J. Phys. Chem. Lett.*, 2012, **3**, 2863-2870.

27. Z. Liu, H. Nie, Z. Yang, J. Zhang, Z. Jin, Y. Lu, Z. Xiao and S. Huang, *Nanoscale*, 2013, **5**, 3283-3288.

28. X. Hu, Y. Wu, H. Li and Z. Zhang, *J. Phys. Chem. C*, 2010, **114**, 9603-9607.

29. T. Ikeda, M. Boero, S. F. Huang, K. Terakura, M. Oshima and J. i. Ozaki, *J. Phys. Chem. C*, 2008, **112**, 14706-14709.

30. P. Lazar, R. Zbořil, M. Pumera and M. Otyepka, *Phys. Chem. Chem. Phys.*, 2014, **16**, 14231-14235.

31. J. Duan, S. Chen, S. Dai and S. Z. Qiao, *Adv. Funct. Mater.*, 2014, **24**, 2072-2078.

32. Y. Kang, X. Ye, J. Chen, Y. Cai, R. E. Diaz, R. R. Adzic, E. A. Stach and C. B. Murray, *J. Am. Chem. Soc.*, 2013, **135**, 42-45.

33. C. Koenigsmann, M. E. Scofield, H. Liu and S. S. Wong, *J. Phys. Chem. Lett.*, 2012, **3**, 3385-3398.

34. M. F. Chisholm, G. Duscher and W. Windl, *Nano Lett.*, 2012, **12**, 4651-4695.

35. Q. M. Ramasse, C. R. Seabourne, D. M. Kepaptsoglou, R. Zan, U. Bangert and A. J. Scott, *Nano Lett.*, 2013, **13**, 4989-4895.

36. M. Audiffred, A. L. Elías, H. R. Gutiérrez, F. López-Urías, H. Terrones, G. Merino and M. Terrones, *J. Phys. Chem. C*, 2013, **117**, 8481-8490.

37. J. Campos-Delgado, I. O. Maciel, D. A. Cullen, D. J. Smith, A. Jorio, M. A. Pimenta, H. Terrones and M. Terrones, *ACS Nano*, 2010, **4**, 1696-1702.

38. B. Delley, *J. Chem. Phys.*, 1990, **92**, 508-517.

39. B. Delley, *J. Chem. Phys.*, 2000, **113**, 7756-7764.

Physical Chemistry Chemical Physics Accepted Manuscript

40. J. P. Perdew, K. Burke and M. Ernzerhof, *Phys. Rev. Lett.*, 1996, **77**, 3865-3868.

41. A. J. Cohen, P. Mori-Sánchez and W. T. Yang, *Chem. Rev.*, 2012, **112**, 289-230.

42. S. Grimme, *J. Comput. Chem.*, 2006, **27**, 1787-1799.

43. D. D. Koelling and B. N. Harmon, *J. Phys. C: Solid State Phys.*, 1977, **10**, 3107-3114.

44. W. Liu, Y. F. Zhu and Q. Jiang, *J. Phys. Chem. C*, 2010, **114**, 21094-21099.

45. W. Gao, X. F. Chen, J. C. Li and Q. Jiang, *J. Phys. Chem. C*, 2009, **114**, 1148-1153.

46. B. Delley, *Mol. Simulat.*, 2006, **32**, 117-123.

47. P. Zhang, B. B. Xiao, X. L. Hou, Y. F. Zhu and Q. Jiang, *Sci. Rep.*, 2014, **4**, 3821.

48. J. A. Keith and T. Jacob, *Angew. Chem. Int. Ed.*, 2010, **49**, 9521-9525.

49. T. Jacob and W. A. Goddard III, *ChemPhysChem*, 2006, **7**, 992-1005.

50. M. J. Janik, C. D. Taylor and M. Neurock, *J. Electrochem. Soc.*, 2009, **156**, B126-B135.

51. V. Tripkovic, E. Skúlason, S. Siahrostami, J. K. Nørskov and J. Rossmeisl, *Electrochim. Acta*, 2010, **55**, 7975-7981.

52. J. Sun, Y. H. Fang and Z. P. Liu, *Phys. Chem. Chem. Phys.*, 2014, **16**, 13733-13740.

53. J. K. Nørskov, J. Rossmeisl, A. Logadottir, L. Lindqvist, J. R. Kitchin, T. Bligaard and H. Jónsson, *J. Phys. Chem. B*, 2004, **108**, 17886-17892.

54. L. Yu, X. Pan, X. Cao, P. Hu and X. Bao, *J. Catal.*, 2011, **282**, 183-190.

55. J. A. Keith, G. Jerkiewicz and T. Jacob, *ChemphysChem*, 2010, **11**, 2779-2794.

Physical Chemistry Chemical Physics Accepted Manuscript

56. S. Kattel and G. Wang, *J. Phys. Chem. Lett.*, 2014, **5**, 452-456.

57. S. Sun, N. Jiang and D. Xia, *J. Phys. Chem. C*, 2011, **115**, 9511-9517.

58. GreeleyJ, I. E. L. Stephens, A. S. Bondarenko, T. P. Johansson, H. A. Hansen, T. F. Jaramillo, J. Rossmeisl, I. Chorkendorff and J. K. Nørskov, *Nat. Chem.*, 2009, **1**, 552-556.

59. X. Pan and X. Bao, *Acc. Chem. Res.*, 2011, **44**, 553-562.

60. D.-H. Lim and J. Wilcox, *J. Phys. Chem. C*, 2012, **116**, 3653-3660.

61. Y. Jiao, Y. Zheng, M. Jaroniec and S. Z. Qiao, *J. Am. Chem. Soc.*, 2014, **136**, 4394-4403.

62. V. Stamenkovic, B. S. Mun, K. J. J. Mayrhofer, P. N. Ross, N. M. Markovic, J. Rossmeisl, J. Greeley and J. K. Nørskov, *Angew. Chem. Int. Ed.*, 2006, **45**, 2897-2901.

Physical Chemistry Chemical Physics Accepted Manuscript